Analysis of mode structure in hollow dielectric waveguide fibers

Mihai Ibanescu, Steven G. Johnson, Marin Soljačić, J. D. Joannopoulos, and Yoel Fink

Center for Materials Science and Engineering and Research Laboratory of Electronics, Massachusetts Institute of Technology,
77 Massachusetts Avenue, Cambridge, Massachusetts 02139

Ori Weisberg, Torkel D. Engeness, Steven A. Jacobs, and M. Skorobogatiy

OmniGuide Communications, One Kendall Square, Building 100 #3, Cambridge, Massachusetts 02139
(Received 10 December 2001; revised manuscript received 22 April 2002; published 17 April 2003)

In this paper, we analyze the electromagnetic mode structure of an OmniGuide fiber—a hollow dielectric waveguide in which light is confined by a large index-contrast omnidirectional dielectric mirror. In particular, we find that the modes in an OmniGuide fiber are similar to those in a hollow metallic waveguide in their symmetries, cutoff frequencies, and dispersion relations. We show that the differences can be predicted by a model based on a single parameter—the phase shift upon reflection from the dielectric mirror. The analogy to the metal waveguide extends to the transmission properties, resulting in the identification of the TE_{01} mode as the lowest-loss mode of the OmniGuide fiber.

I. INTRODUCTION

The advent of high-purity ultra-low-loss silica fiber as a transmission medium in the late 1970s provided a basis for the modern optical communication infrastructure. Although highly successful, silica waveguides have fundamental limitations in their attenuation and nonlinearities that result from the interaction of light with a dense, material-filled core. A different approach to waveguiding circumvents these problems by confining light in a hollow core using highly reflective walls. This approach is exemplified by hollow metallic waveguides that are very efficient in the millimeter wavelength range. Prior to the emergence of silica fiber, these waveguides were seriously considered as candidate media for long-distance telecommunications [1]. An impairment of metallic waveguides is that they become lossy at high frequencies due to the finite conductivity of metals. Thus, their use is restricted to low frequencies. This severely limits the ultimate bandwidth that they can transmit. By adding a dielectric coating on the inside of the metallic waveguide one can improve its properties. Such metallodielectric waveguides have been developed for infrared wavelengths, in particular, for laser power delivery [2,3].

Here we analyze an OmniGuide fiber—a hollow *all-dielectric* waveguide in which light is confined by an omnidirectional mirror [4]. The limitations that exist in both the silica fiber and the hollow metal waveguides can be systematically reduced in this waveguide due to its hollow core and the use of dielectric materials transparent at high frequencies.

Yeh *et al.* showed in 1978 that it is possible to transmit a non-index-guided mode in a multilayer cylindrical dielectric waveguide [5]. The radiative decay of the mode is suppressed using a Bragg reflector, i.e., a multilayered structure that is periodic in the radial direction. Initial work in this area has been focused on structures based on doped-silica technology that have a low index contrast between the layers [6–9]. These structures are useful, for example, to control the dispersion parameter of a fiber in ways that are not achievable in a standard silica fiber [9]. However, such structures cannot confine light primarily in a hollow core because

of the large penetration of the field into the low index-contrast multilayer structure. Recently, with the discovery of the omnidirectional high-reflectivity properties of multilayer films [10–12], researchers have focused instead on high index-contrast dielectric waveguides [4,13–18]. Fink *et al.* fabricated a large-core high index-contrast hollow dielectric waveguide and demonstrated that light is transmitted even when tight bends are introduced in the waveguide, a result of the omnidirectionality of the dielectric mirror [13]. Xu *et al.* developed an efficient analytical method for calculating approximate dispersion relations of the modes of such waveguides, making use of the radial periodicity of the cladding layers [14]. Using this method, they calculated the number of layers required to suppress radiation as a function of the index contrast and substantiated that a large index contrast is necessary in order to limit the number of layers to a reasonable value [15]. Ibanescu *et al.* exploited the similarities between a dielectric multilayer mirror and a metal mirror and showed that it is possible to design an all-dielectric coaxial waveguide that supports a TEM-like mode [17].

In this paper, we will study the properties of a hollow dielectric waveguide in which light is confined by a large index-contrast omnidirectional dielectric mirror. The large index contrast produces a high degree of optical confinement in the core and results in a waveguide mode structure that is very similar to the mode structure of a hollow metallic waveguide. We present the similarities and differences between the hollow dielectric and metallic waveguides, and explain these results using a single-parameter model based on the phase shift upon reflection from the dielectric mirror. In addition, we show that the similarities between these two types of waveguides extend to their transmission properties, in which they have the same lowest-loss mode, the TE_{01} mode.

II. HOLLOW WAVEGUIDES

The waveguides that we compare are shown in Fig. 1. On the left is depicted an OmniGuide fiber. A hollow core (index of refraction $n_0 = 1$) is surrounded by an omnidirectional mirror that consists of alternating layers having high and low
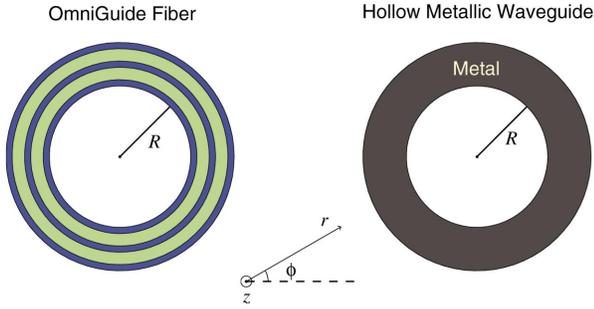
FIG. 1. (Color) (Left) OmniGuide fiber of radius R. Light is confined in the hollow core by a multilayer dielectric mirror made of alternating layers with high (blue) and low (green) indices of refraction. (Right) Hollow metallic waveguide of radius R. Light is confined in the hollow core by a metallic cylinder.

FIG. 2. (Color) (Left) Projected band structure associated with the dielectric mirror. The blue regions correspond to (β,ω) pairs for which light can propagate through the mirror. The meaning of the parallel wave vector β is shown in the inset. k_T is the transverse component of the wave vector. The diagonal black line represents the light line ($\omega = c\beta$). Shown in gray are two frequency ranges corresponding to omnidirectional reflectivity of the mirror. (Right) Frequency cutoffs of the lowest 11 modes supported by a hollow metallic waveguide are plotted versus the radius of the waveguide. TE polarized modes are shown in red, while TM modes are shown in blue. The number m in the labels is the angular momentum index of each mode. Note the degeneracy of the TE_{01} and the TM_{11} modes. The two thick vertical dashed lines correspond to radii $R = 2.0a$ and $R = 3.8a$, which are the values used for the two exemplary waveguides in this paper.

indices of refraction [10]. The high and low indices of refraction layers are shown in blue and green, respectively. The indices of refraction are 4.6 and 1.6 with corresponding thickness $0.33a$ and $0.67a$, where a is the total thickness of a pair of layers. These values for the indices of refraction have been used in previous works [4,10,13–15,17], including a fabricated multilayered waveguide operating at 10.6 μm. The large index contrast between the two types of layers allows us to better illustrate the comparison between the hollow dielectric and metallic waveguides; the conclusions are still valid for a smaller index contrast that one may have to use in practice. In the frequency range of omnidirectionality of the dielectric mirror, the similarities between the two types of waveguides are enhanced because, in both cases, the mirror that confines light in the core is a very good reflector *for all angles of incidence and polarizations*. Moreover, the omnidirectionality of the dielectric mirror is important for practical considerations: in an imperfect waveguide, the coupling between the operating core mode and cladding modes above the light line is eliminated if the frequency of operation lies in the omnidirectional frequency range of the mirror.

The exact value of black a in microns is determined by the wavelength of operation of the waveguide. For example, if one wants to use $\lambda = 1.55$ μm, then the thickness of a bilayer should be chosen somewhere in the range $a = 0.3 - 0.4$ μm. The radius R of the waveguide will vary in the different examples presented in this paper from a minimum of $2a$ to a maximum of $20a$.

On the right side of Fig. 1, we show a hollow metal waveguide. The core is the same as in the OmniGuide fiber (index of refraction 1, radius R), but a perfectly conducting metal cylinder now replaces the multilayer cladding.

We expect the multilayer structure to confine light in the core of the waveguide in a frequency range that corresponds to the band gap of a planar multilayer mirror having the same parameters as those of the multilayer structure in the waveguide. Indeed, it is precisely in this band-gap region that we expect the mode structure of the OmniGuide fiber to resemble that of a hollow metal waveguide.

In the left panel of Fig. 2, we plot the projected band structure for a planar multilayer dielectric mirror, for which the layers have the same indices of refraction and the same

thicknesses as those of the layers present in the waveguide. If ω is the frequency of an incoming plane wave and β is the component of the wave vector parallel to the mirror, then regions in the (β,ω) plane shown in blue correspond to plane waves that can couple to propagating modes in the mirror and are transmitted through the mirror. The two gray areas in the plot correspond to the omnidirectional frequency ranges of the dielectric mirror. For these frequencies, light cannot be transmitted through the mirror for any angle of incidence of a plane wave incoming from the outside air region. Both the TE and TM polarizations are overlapped in the plot.

In the right panel of Fig. 2, the frequency cutoffs of the lowest 11 modes supported by a hollow metallic waveguide are plotted versus the radius of the waveguide. The dispersion relation of a mode with cutoff frequency ω_c is given by $\omega^2 = c^2\beta^2 + \omega_c^2$. TE polarized modes are shown in red, while TM modes are shown in blue. The number m in the labels is the angular momentum of each mode. Note the degeneracy of the TE_{01} and the TM_{11} modes. The two vertical dashed lines correspond to radii $R = 2.0a$ and $R = 3.8a$, which are the values used for the OmniGuide fibers that we analyze.

III. CALCULATION OF MODES OF THE OMNIGUIDE FIBER

We calculate the modes supported by the OmniGuide fiber using the transfer-matrix method. As in any waveguide

with cylindrical symmetry, there are three useful conserved quantities: ω, the frequency; β, the wave vector in the axial direction; and m, the angular momentum ($m = 0,1,2,\dots$). The general form of the z component of the electric field, E_z, in the ith layer of the structure for a mode with wave vector β and angular momentum m is

$$E_z(z,r,\phi) = [A_i J_m(k_{T,i}r) + B_i Y_m(k_{T,i}r)]e^{i(\beta z - \omega t)}e^{im\phi}, \quad (1)$$

where A_i and B_i are coefficients that vary from layer to layer, J and Y are Bessel functions, and $k_{T,i}$ is the transverse wave vector, $k_{T,i} = \sqrt{(n_i \omega/c)^2 - \beta^2}$. H_z is given by a similar expression, but with different coefficients C_i and D_i. From the E_z and H_z components one can calculate all the other components of the electromagnetic field components [19]. The coefficients in the $(i+1)$th layer are related to those in the ith layer by a 4×4 transfer matrix such that the boundary conditions are satisfied [5]. The last step before finding the modes is to establish boundary conditions at the outside surface of the outermost layer. Here we require that the incoming radial electromagnetic flux be zero, which corresponds to the physical situation in which the sources of electromagnetic field are only inside the waveguide [4]. The solutions that we obtain with this boundary condition are guided modes (with real wave vectors) and leaky modes (with complex wave vectors).

The OmniGuide fiber supports modes that are analogous to the guided modes of a hollow metallic waveguide. These modes are resonant modes that have most of their energy traveling in the hollow core. Their field decays exponentially in the radial direction in the dielectric layers. These modes have (β,ω) pairs situated at the band gap of the dielectric mirror and above the light line. The wave vector β has an imaginary part that is proportional to the radiative loss of the modes. This imaginary part decreases exponentially with the number of layers in the dielectric mirror; in the limit of an infinite number of layers these resonant modes become truly guided modes. For the dielectric mirror with only five layers shown in Fig. 1, the imaginary part is of the order of $10^{-4} \times 2\pi/a$. This means that light can be confined in the hollow core for a distance equal to several hundred wavelengths before it radiates away. For a waveguide intended for transmission of light over longer distances, more layers need to be added to the cladding. Fortunately, the imaginary part of the wave vector decreases exponentially with the increase in the number of layers. Thus, for pure TE modes, only 20 layers are enough to give radiative decay lengths of more than a 100 km while for TM modes and mixed modes, 40 layers are enough. For a detailed analysis of radiation suppression, see Refs. [4,15].

The OmniGuide fiber also supports other categories of modes. One category includes modes that are index guided in the dielectric mirror. In Fig. 2, these modes are situated below the light line, in the light-blue regions of the $\omega(\beta)$ diagram. Their field decays exponentially in the air regions, but extends throughout the dielectric mirror. Another category includes modes that decay both in the air regions and in the dielectric layers. These only exist as surface states
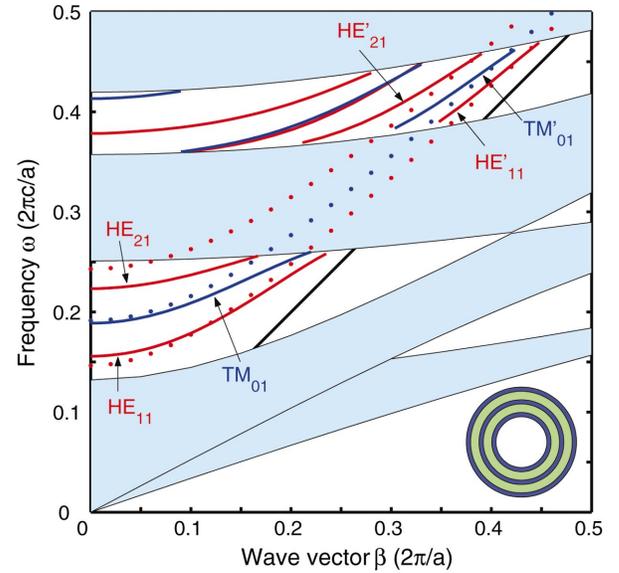
FIG. 3. (Color) Modes supported by an OmniGuide fiber of radius $R = 2.0a$ are shown with solid lines. Red is for TE and HE modes, while blue is for TM and EH modes. Only the first three modes are labeled in each band gap. The lowest three modes in a hollow metallic waveguide with the same radius are plotted as dots.

between the core and the multilayer cladding. (They can also be found deeper in the multilayer structure if a defect is introduced by altering the thickness or the index of refraction of one or more layers). In Fig. 2, these modes are situated below the light line in the band gap of the dielectric mirror.

IV. COMPARISON OF OMNIGUIDE FIBER MODES AND METAL WAVEGUIDE MODES

In Fig. 3, we show the lowest-frequency resonant modes of the OmniGuide fiber for a radius $R = 2.0a$. TE modes and TE-like (HE) modes are shown as solid red lines, while TM and TM-like (EH) modes are shown as solid blue lines. The modes of a hollow metallic waveguide with the same radius are shown as dots. The figure shows that, indeed, the dispersion relations of the OmniGuide fiber are very similar to those of the metallic waveguide, but the modes can now only exist in the TE or TM band gaps of the multilayer mirror. For example, the TM_{01} mode in the metallic waveguide (blue dots) is now split into two submodes, TM_{01} and TM'_{01}. Thus, it is useful, in a zeroth-order approximation, to think that the dispersion relations for the different modes of the OmniGuide fibers can be obtained by overlapping the band structure of the dielectric mirror on top of the dispersion relations for the metallic waveguide. Finally, we note that it is possible for resonant modes to exist outside the omnidirectional frequency range [such as the HE_{11} mode for $\beta < 0.05(2\pi/a)$ in Fig. 3] as long as the modes fall within the band gap.

In Fig. 4, we show the dispersion relations for a larger radius of the fiber, $R = 3.8a$. More resonant modes can be found now in the first band gap as the cutoff frequencies vary inversely with the radius R. We focus on the first band gap of the dielectric mirror, and we consider only the lowest five resonant modes of the waveguide.
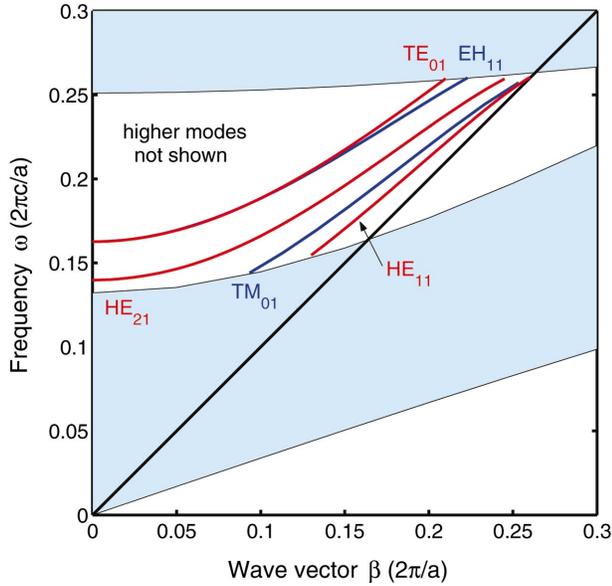
FIG. 4. (Color) The lowest five modes supported by an Om-niGuide fiber of radius $R = 3.8a$ are shown as solid red (TE or TE-like modes) and blue (TM or TM-like modes) curves. Higher modes exist, but are not shown.

FIG. 5. (Color) The electric-field time-average energy density for the five modes in Fig. 4 is shown in a transverse cross section of the waveguide. The color scheme is such that the energy density goes from zero (black) to maximum (yellow). The thin blue con-tours represent the contours between the different layers of the Om-niGuide fiber. For all five modes, the energy density is plotted for a frequency $\omega = 0.230(2\pi/a)$.

We will compare the resonant modes shown in Figs. 3 and 4 with the modes in metal waveguides of corresponding radii ($R = 2.0a$ and $R = 3.8a$). In particular, we will compare the resonant modes to the metal waveguide modes in terms of their cutoff frequencies, group velocities, group velocity dis-persions, degeneracies, and mode symmetries. The lowest resonant mode in Fig. 3 is HE_{11} with a cutoff frequency $\omega = 0.155(2\pi/a)$. This corresponds to TE_{11}, the fundamental mode in a hollow metal waveguide, which has a cutoff at $\omega = 0.146(2\pi/a)$. The second mode in Fig. 3 is TM_{01} with $\omega = 0.189(2\pi/a)$, corresponding to TM_{01} in the metal wave-guide with $\omega = 0.191(2\pi/a)$. Note that for $m = 0$ modes, the OmniGuide fiber modes are exactly TE or TM polarized, as is the case with all-metal waveguide modes. For nonzero m, TE modes become HE modes, and TM modes become EH modes. Also, in both waveguides, the nonzero m modes are doubly degenerate, while the $m = 0$ are nondegenerate.

In Table I, we summarize the similarities between the equivalent modes in the OmniGuide fiber and the hollow

TABLE I. Summary of comparison between OmniGuide fiber (OGF) modes and their hollow metallic waveguide (HMW) coun-terparts. The first three modes are taken from Fig. 3 for a radius $R = 2.0a$, and the next two are from Fig. 4, corresponding to $R = 3.8a$.

Mode label		Cutoff frequency			Degeneracy	
OGF	HMW	OGF	HMW	Difference	OGF	HMW
HE_{11}	TE_{11}	0.155	0.146	+6%	2	2
TM_{01}	TM_{01}	0.189	0.191	−1%	1	1
HE_{21}	TE_{21}	0.223	0.243	−8%	2	2
EH_{11}	TM_{11}	0.163	0.160	+2%	2	2
TE_{01}	TE_{01}	0.163	0.160	+2%	1	1

metallic waveguide. The first three modes are taken from Fig. 3 for a radius $R = 2.0a$, and the next two are from Fig. 4, corresponding to $R = 3.8a$. The cutoff frequencies for the two types of waveguides are quite similar for all the five modes. The differences vary from -8% for the HE_{21} mode to $+6\%$ for the TM_{01} mode. Also note that the modes in the metal waveguide having low cutoff frequencies [below $0.18(2\pi/a)$] are shifted up in the OmniGuide fiber, while metallic modes with higher cutoff frequencies are shifted down. This effect will be explained later in terms of the phase shift of the dielectric mirror.

The group velocity of a resonant mode is zero at $\beta = 0$ and approaches c as the frequency is increased, as is the case in a metal waveguide. However, as the mode nears the upper band edge, the group velocity starts decreasing as a result of the gradual loss of confinement in the core.

The group velocity dispersion of a resonant mode is posi-tive for low frequencies (closer to the lower edge of the band gap), negative for high frequencies and transitions through zero. This is in contrast to the group velocity dispersion of modes in a metal waveguide, which is always positive.

To provide a better understanding of the field patterns of OmniGuide fiber modes, in Fig. 5 the electric-field time-average energy density $\frac{1}{2}\varepsilon|\vec{E}|^2$ is plotted for the five modes shown in Fig. 4 at a frequency $\omega = 0.230(2\pi/a)$. All modes are normalized such that the power flowing in the z direction is the same. Also, in order to capture the angular dependence of a mode, we no longer use the $e^{im\phi}$ complex form of the field. Instead, we use linear combinations of the degenerate m and $-m$ modes to obtain real fields.

All modes appear to be very well confined to the hollow core. The energy density in the cladding layers is much smaller than the energy density in the core, which is why the cladding layers appear dark in the figure. The TE_{01} mode is different from the other four modes, in which its electric-field energy density has a node near the core-mirror inter-face. This is true, in general, for all modes of the same sym-

metry, i.e., $TE_{0\ell}$ with $\ell = 1, 2, \ldots$. Note that the number of angular oscillations of the energy density is twice the angular momentum of a mode.

In order to quantify the comparison between the field distribution of modes in the OmniGuide fiber and in the metal waveguide, we use a correlation function Γ defined by

$$\Gamma = \frac{\left| \int r \, dr \, d\phi \, \vec{E}_1(r, \phi) \cdot \vec{E}_2(r, \phi) \right|}{\left[\int r \, dr \, d\phi \, |\vec{E}_1(r, \phi)|^2 \int r \, dr \, d\phi \, |\vec{E}_2(r, \phi)|^2 \right]^{1/2}}. \quad (2)$$

Γ can take values in the interval $[0,1]$, a value of 1 corresponding to maximum correlation ($\Gamma = 1$ can only happen if the two modes are the same up to a constant amplitude scaling factor). For all modes, the correlation is largest, close to the middle of the band gap and decreases as the mode approaches the band edges. The maximum value of the correlation as a function of frequency is above 95% for all modes, and the largest correlation is found for the TE_{01} mode, i.e., 99.1%.

V. PHASE-SHIFT MODEL

In both the hollow metallic waveguide and the OmniGuide fiber, light is confined in the air region because it is reflected back to the core by a cladding: a metal wall in the first case and a dielectric multilayer film in the second. Thus, it is convenient to analyze the differences between the modes in the two waveguides in terms of the different reflection properties of the two mirrors. Since the reflectivity is very close to 100% in both cases, the important difference between the two mirrors is found in the phase shift $\Delta\phi$ acquired by an electromagnetic wave upon reflection. For the TE polarization, this phase shift is defined by

$$\frac{E_r^{\parallel}}{E_i^{\parallel}} = e^{i\Delta\phi}, \quad (3)$$

where $E_i^{\parallel}$ and $E_r^{\parallel}$ are the tangential components of the electric field for the incident and reflected waves, respectively. In the above formula, we assume that the reflectivity is 100%, which is true for a perfectly conducting wall and is a very good approximation for a dielectric mirror with a large enough number of layers. For a metallic mirror, $\Delta\phi$ is always equal to π because the tangential electric fields of the incident and reflected waves have to cancel. For the TM polarization, we calculate $\Delta\phi$ in a similar manner by using the tangential components of the magnetic field this time: $H_r^{\parallel}/H_i^{\parallel} = -e^{i\Delta\phi}$. With this definition, $\Delta\phi$ for a metal mirror is equal to π for all polarizations and angles of incidence.

In Fig. 6, we plot the phase shift of the dielectric mirror as contours on a plot, which includes the band-gap edges, the light line, and dispersion relations for the fiber with $R = 2.0a$. The phase shift is a function of ω and β, or, equivalently, of the frequency and the angle of incidence. Also, it is a function of the polarization of the incident wave. For both polarizations, we can identify a $\Delta\phi = \pi$ line near the center
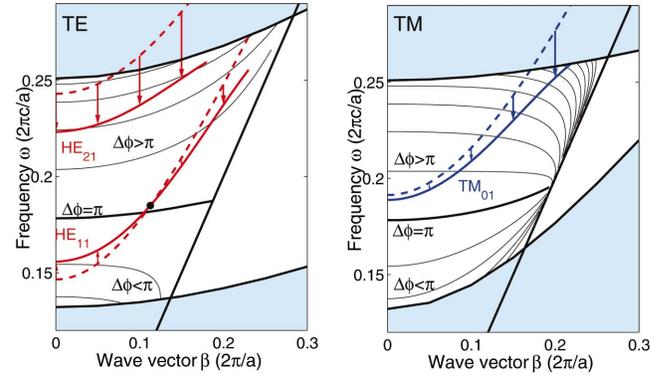
FIG. 6. (Color) Combined phase-shift and dispersion relation diagrams. Left panel: contour lines for the phase shift $\Delta\phi$ are plotted together with the band gap of the dielectric mirror (white region), and the light line (black oblique line). The modes of the OmniGuide fiber with $R = 2.0a$ are shown as solid red and blue lines for TE and TM-like modes, while the modes in the metal waveguide are shown as dotted lines. The vertical arrows show the frequency difference between equivalent modes in the waveguides. The left and right panels are for modes with TE-like and TM-like polarization, respectively. The crossing between the OmniGuide HE_{11} mode and the metallic TE_{11} mode is shown as a black dot.

of the band gap (shown with a thicker black line). This is where we expect the dielectric mirror to be most similar to a metal mirror. The other contour lines correspond to phase shifts of 1.1π, 1.2π, $\ldots$ for increasing frequencies, and 0.9π, 0.8π, $\ldots$ for decreasing frequencies. The qualitative difference between the two polarizations is that for the TE polarization the phase shift at a given frequency approaches π near the light line, whereas for the TM polarization it varies substantially near the light line.

Also shown in Fig. 6 are the confined modes for the metallic waveguide (dashed lines) and for the OmniGuide fiber (solid lines). On the left we present TE-like modes, while on the right the pure TM mode is shown.

As seen in Fig. 6, the difference in the dispersion curves for the confined modes in the metallic waveguide and the OmniGuide fiber are correlated with the difference in phase shifts between the dielectric and metal mirrors. In particular, the following observations can be made.

(i) The point of crossing between the mode and the metallic TE_{11} mode lies very close to the $\Delta\phi = \pi$ line.

(ii) The frequency distance between the equivalent modes in the metal and dielectric waveguides increases as the phase shift of the dielectric mirror moves away from $\Delta\phi = \pi$.

(iii) The confined modes in the dielectric waveguide are drawn towards the $\Delta\phi = \pi$ line when compared with the modes confined in the metal waveguide.

Next we present a simple model that explains qualitatively the above observations by relating the phase shift to the dispersion curves. We approximate the transverse field profile of a confined mode of the OmniGuide fiber by a standing wave between two planar walls separated by the diameter of the waveguide. The total phase acquired by a wave that traverses the waveguide diameter twice has contributions from propagation over a distance $2(2R)$ and from two reflections upon the mirror. Thus,

$$\Delta\phi_{total} = 4k_T R + 2\Delta\phi, \qquad (4)$$

where k_T is the transverse wave vector of the mode in core. The condition for a standing wave is that this phase must equal a multiple of 2π: $\Delta\phi_{total} = 2\ell\pi$. This in turn leads to the approximate dependence of the transverse wave vector on the phase shift,

$$k_T = (\ell\pi - \Delta\phi)/(2R). \qquad (5)$$

Calculating k_T from this equation should be done self-consistently because $\Delta\phi$ is a function of ω and β, and therefore a function of k_T.

From Eq. (5) we see that why the phase shift $\Delta\phi$ has important effects on the dispersion relations of modes. Since k_T is a decreasing function of $\Delta\phi$, and because $\omega^2/c^2 = \beta^2 + k_T^2$, it follows that an increase in the phase shift $\Delta\phi$ will cause a decrease in the frequency ω of a mode at a fixed wave vector β. This result explains the three qualitative observations made above about the OmniGuide modes when compared to the metallic waveguide modes.

The most important and visible difference between the two sets of modes is that the OmniGuide modes are pulled inside the band gap when compared to their metallic counterparts. This is entirely due to the fact that the phase shift increases with increasing frequency. One consequence is that the group velocity of the OmniGuide modes is always slightly smaller than that of the corresponding metallic modes. It is interesting to imagine what would happen if one could design a multilayer dielectric mirror for which the phase shift decreased with increasing frequency: in such a waveguide, the modes would be pulled out towards the band-gap edges, leading to modes with larger group velocities that could approach the upper bound of c. However, it is an empirical law that the phase shift always has the general behavior shown in Fig. 6. Finally, we note that the point of maximum correlation between OmniGuide fiber modes and metallic modes, as defined above, occurs very close to the $\Delta\phi = \pi$ line.

VI. SPECIAL CHARACTERISTICS OF THE TE$_{01}$ MODE

For practical applications, it is of interest to identify the losses associated with the different modes of the waveguide. Metallic waveguides were the subject of intensive research aimed at utilizing them for long-distance optical communications. It was found that the TE$_{01}$ mode is the lowest-loss mode in a metal waveguide due to the presence of a node in the electric field at the metallic wall. This mode was the operating mode for the long-distance communication lines designed by the Bell Laboratories prior to the advent of silica fibers [1]. In the remaining portion of this paper, we will examine some of the properties of the TE$_{01}$ mode in the OmniGuide fiber; these properties were studied in more detail in Ref. [4].

In the left panel of Fig. 7, we plot the confinement in percent of the electromagnetic energy in the core for the TE$_{01}$, TM$_{01}$, and HE$_{11}$ modes as a function of the core radius for a fixed frequency $\omega = 0.256(2\pi/a)$. As shown, the
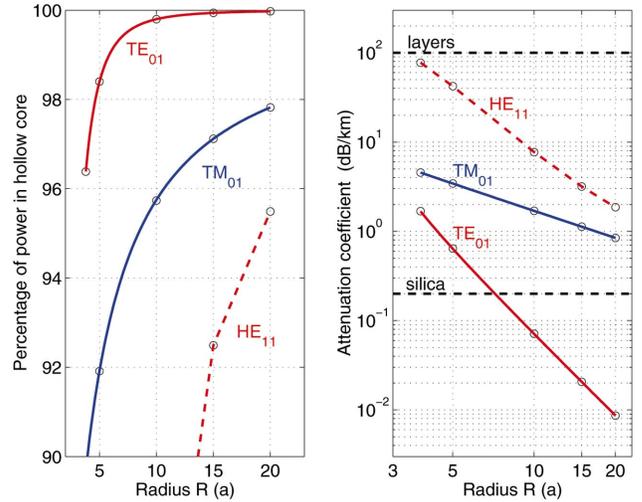
FIG. 7. (Color) (Left) The confinement of electromagnetic energy in the hollow core of the OmniGuide fiber is plotted for three modes as a function of core radius. Actual data is shown as open circles. The solid lines represent fits as discussed in the text, and the dashed line is simply connecting the data points. (Right) The attenuation coefficient of the three modes is plotted as a function of radius. Also shown are the attenuation coefficient in silica fibers (0.2 dB/km) and a much larger attenuation coefficient (100 dB/km) assumed for the materials in the multilayer mirror. The circles and the lines have the same significance as in the left panel.

TE$_{01}$ mode has the largest confinement for all values of R. Furthermore, its confinement in the core approaches 100% at a faster rate than the other modes. The penetration of the TE$_{01}$ field into the multilayer structure is very well approximated by a $1/R^3$ dependence. We present a justification for the $1/R^3$ dependence in the Appendix. A fit to the actual data points (open circles) is shown in Fig. 7 as a solid red line. The TM$_{01}$ confinement approaches 100% at a much slower rate. A fit with a $1/R^3$ dependence is shown as a solid blue line. The HE$_{11}$ mode has a mixed polarization and has a more complex variation with the core radius. However, the rate at which its confinement approaches 100% is less than that of the TE$_{01}$ mode.

In the right panel of Fig. 7, we plot the attenuation coefficient caused by dissipation losses for the three modes. (We assume that the dielectric mirror has enough layers such that the radiation losses are negligible). We assume the core of the waveguide is lossless, while the materials in the dielectric mirror have a dissipation coefficient of 100 dB/km (chosen to much larger than the loss of silica). Even with such lossy materials in the dielectric mirror, the loss of the TE$_{01}$ mode is smaller than the loss of silica fibers (0.2 dB/km) if the core radius R is larger than $\approx 8a$. This is because the dissipation loss for TE$_{0\ell}$ ($\ell = 1, 2, \dots$) modes decreases as $1/R^3$. This general result is a consequence of the presence of a node in the electric field near the core-mirror interface. We present a more detailed justification in the Appendix. Note that while the silica fiber has a very low loss only for wavelengths near $\lambda = 1.55\ \mu$m, the OmniGuide fiber can be designed to have a very low loss in the vicinity of any desired wavelength, from infrared to visible wavelengths.

TE$_{01}$ is the lowest-loss mode within the TE$_{0\ell}$ family of modes. From the derivation presented in the Appendix one can show that the loss of a TE$_{0\ell}$ mode is proportional to the square of the transverse wave vector in the core, $k_{T,core}$. This implies a monotonic increase of the loss with the order ℓ. In particular, the loss of TE$_{02}$ is about 3.3 times larger than that of TE$_{01}$ for almost all frequencies and core radii.

For modes other than the TE$_{0\ell}$ modes, the absence of the node in the electric field near the core-layer interface results in more penetration of the field into the cladding, and also different scaling laws for the R dependence. Turning back to Fig. 7, we see that the TM$_{01}$ dissipation loss follows exactly a $1/R$ dependence (solid blue line), while the loss of HE$_{11}$ has some intermediate dependence with a slope that approaches $1/R$ for large R.

Another reason for the low losses of the TE$_{01}$ mode is the fact that this mode is confined in the core only by the TE gap. TM modes and mixed modes have a component that is confined by the weaker TM gap, and thus they penetrate deeper into the multilayer cladding.

The fact that the TE$_{01}$ loss is smaller than that of the other modes is very important for the transmission properties of OmniGuide fibers. Even if several modes are excited at the input of a waveguide, after a certain distance only the TE$_{01}$ mode will remain in the waveguide. This loss-induced modal discrimination results in an effectively single-mode operation in a waveguide that supports many modes. In our analysis, we assumed that the number of layers in the dielectric mirror is large enough such that radiation losses can be neglected. By choosing the number of layers appropriately, the loss-induced modal discrimination can be further enhanced since the radiation losses are also the smallest for TE$_{01}$ [4,5,8].

While the radiation and absorption losses of the TE$_{01}$ decrease substantially when the core radius is increased, the analysis of attenuation in a practical waveguide necessitates the consideration of other loss mechanisms. In particular, the loss of the TE$_{01}$ mode is increased by coupling to other resonant modes or to cladding modes due to deviations from a straight and perfect waveguide. These effects are analyzed in detail in Ref. [4].

VII. CONCLUSIONS

In conclusion, we have shown that the mode structure of an OmniGuide fiber has many similarities with that of a hollow metallic waveguide. We explained why these similarities exist, and we presented a simple model that accounts for the differences. We identified the TE$_{01}$ mode as the lowest-loss mode in the dielectric waveguide, as it was the case for the metal waveguide. It is hoped that the analogy developed in this paper has provided an intuitive understanding of the modal structure of the OmniGuide fiber and could be applied to the design of transmission lines or optical devices based on this type of fiber.

ACKNOWLEDGMENTS

APPENDIX: DEPENDENCE OF TE$_{01}$ ABSORPTION LOSSES ON CORE RADIUS

The $1/R^3$ dependence of the TE$_{01}$ dissipation loss is due to the presence of a node in the electric field of this mode near the interface between the hollow core and the first layer of the dielectric mirror. The only nonzero component of the electric field for the TE$_{01}$ mode is E_ϕ. In the case of a metallic waveguide, this component would be exactly zero at the interface between the hollow core and the metal. In the case of the dielectric waveguide, the node in E_ϕ is found very close to the interface.

To get an estimate of the dissipation losses, we take the ratio of the power that travels in the layers to the total power carried by the mode [20]. Let A_{core} be the amplitude of the electric field in the core, and A_{layers} the amplitude in the layers. The area of the core is πR^2. Due to the exponential radial decay induced by the band gap, the power in the layers is found mostly in the first few layers, in an area approximately equal to $2\pi R d_p$ (d_p is the penetration depth of the field into the layers and is independent of R). With these notations, the estimate for the loss coefficient $\mathcal{L}$ is

$$\mathcal{L} \sim \frac{A_{layers}^2 2\pi R d_p}{A_{core}^2 \pi R^2} \sim \frac{1}{R}\left(\frac{A_{layers}}{A_{core}}\right)^2, \tag{A1}$$

where we kept only terms that influence the R dependence.

Due to the small amplitude of E_ϕ at the core-layer interface, it is the derivative of E_ϕ with respect to r that connects the amplitudes A_{layers} and A_{core}. If we approximate the radial field oscillations by sinusoidal oscillations, the derivative of E_ϕ close to a node is given by the transverse wave vector times the amplitude of E_ϕ. Thus, the amplitudes in the core and in the layers are connected by $k_{T,core}A_{core} \simeq k_{T,layers}A_{T,layers}$. The transverse wave vector $k_{T,core}$ is inversely proportional to R because the TE$_{01}$ mode always has half an oscillation of E_ϕ between the origin and $r=R$. In a layer with index of refraction n, we have $k_T = \sqrt{(n\omega/c)^2 - \beta^2}$. As R becomes larger, the TE$_{01}$ mode will get closer to the light line, and therefore β approaches ω/c. If n is not equal to 1, k_T will be almost independent of R. Thus $k_{T,layers}$ is almost independent of R. Thus, we have

$$\frac{A_{layers}}{A_{core}} \simeq \frac{k_{T,core}}{k_{T,layers}} \sim \frac{1}{R}. \tag{A2}$$

The expression for the loss becomes

$$\mathcal{L} \sim \frac{1}{R}\left(\frac{A_{layers}}{A_{core}}\right)^2 \sim \frac{1}{R^3}, \tag{A3}$$

which is the result we wanted to justify.

[1] W.D. Warters, Bell Syst. Tech. J. **56**, 1825 (1977).

[2] M. Miyagi and S. Kawakami, J. Lightwave Technol. **LT-2**, 116 (1984).

[3] Y. Matsuura and J.A. Harrington, J. Opt. Soc. Am. A **14**, 1255 (1997).

[4] S.G. Johnson, M. Ibanescu, M. Skorobogatiy, O. Weisberg, T.D. Engeness, M. Soljacic, S.A. Jacobs, J.D. Joannopoulos, and Y. Fink, Opt. Express **9**, 748 (2001).

[5] P. Yeh, A. Yariv, and E. Marom, J. Opt. Soc. Am. **68**, 1196 (1978).

[6] N.J. Doran and K.J. Bulow, J. Lightwave Technol. **LT-1**, 588 (1983).

[7] A.N. Lazarchik, Radiotekh. Elektron. (Moscow) **1**, 36 (1988).

[8] C.M. de Sterke and I.M. Bassett, J. Appl. Phys. **76**, 680 (1994).

[9] F. Brechet, P. Roy, J. Marcou, and D. Pagnoux, Electron. Lett. **36**, 514 (2000).

[10] Y. Fink, J.N. Winn, S. Fan, C. Chen, J. Michel, J.D. Joannopoulos, and E.L. Thomas, Science **282**, 1679 (1998).

[11] J.N. Winn, Y. Fink, S. Fan, and J.D. Joannopoulos, Opt. Lett. **23**, 1573 (1998).

[12] D.N. Chigrin, A.V. Lavrinenko, D.A. Yarotsky, and S.V. Gaponenko, Appl. Phys. A: Mater. Sci. Process. **68**, 25 (1999).

[13] Y. Fink, D.J. Ripin, S. Fan, C. Chen, J.D. Joannopoulos, and E.L. Thomas, J. Lightwave Technol. **17**, 2039 (1999).

[14] Y. Xu, R.K. Lee, and A. Yariv, Opt. Lett. **25**, 1756 (2000).

[15] Y. Xu and A. Yariv, in *Proceedings of the SPIE*, edited by A. Dutta, A.A.S. Awwal, N. K. Dutta, and K. Okamoto (SPIE-Int. Soc. Opt. Eng., Washington, 2001), Vol. 4532, pp. 191–205.

[16] T. Kawanishi and M. Izutsu, Opt. Express **7**, 10 (2000).

[17] M. Ibanescu, Y. Fink, S. Fan, E.L. Thomas, and J.D. Joannopoulos, Science **289**, 415 (2000).

[18] A. Argyros, Opt. Express **10**, 1411 (2002).

[19] J.D. Jackson, *Classical Electrodynamics*, 3rd ed. (Wiley, New York, 1998).

[20] A more precise expression is derived in Ref. [4], but the proof of the $1/R^3$ dependence is the same.